

ARTICLE

Open Access

# Nature-inspired rollable electronics

Gunhee Lee<sup>1,2</sup>, Yong Whan Choi<sup>1,3</sup>, Taemin Lee<sup>1,2</sup>, Kyung Seob Lim<sup>4</sup>, Jooyeon Shin<sup>1,2</sup>, Taewi Kim<sup>5</sup>, Hyun Kuk Kim<sup>6</sup>, Bon-Kwon Koo<sup>7,8</sup>, Han Byul Kim<sup>9</sup>, Jong-Gu Lee<sup>2</sup>, Kihyeon Ahn<sup>5</sup>, Eunhan Lee<sup>5</sup>, Min Suk Lee<sup>10</sup>, Jin Jeon<sup>10</sup>, Hee Seok Yang<sup>10</sup>, Phillip Won<sup>2</sup>, Seongho Mo<sup>11</sup>, Namkeun Kim<sup>11</sup>, Myung Ho Jeong<sup>12</sup>, Yeonwook Roh<sup>5</sup>, Seungyong Han<sup>5</sup>, Je-Sung Koh<sup>5</sup>, Sang Moon Kim<sup>11</sup>, Daeshik Kang<sup>5</sup> and Mansoo Choi<sup>1,2</sup>

## Abstract

Inspired by the rolling mechanism of the proboscis of a butterfly, rollable electronics that can be rolled and unrolled to a great extent on demand are developed. Generally, electronic devices that are attached to various surfaces to acquire biosignals require mechanical flexibility and sufficient adhesive force. The rollable platform provides sufficient force that grips onto the entire target surface without destroying the target organ. To prove the versatility of our device not only in gripping and detecting biosignals from micro objects but also in performing a variety of functions, thin-film electronics including a heater, strain sensor and temperature sensor are constructed on the rollable platform, and it is confirmed that all the electronics operate normally in the rolled and unrolled states without breakdown. Then, micro bio-objects are gripped by using the rollable platform, and their tiny motions are successfully detected with the sensor on the platform. Furthermore, the detection of the pulse wave signals of swine under diverse experimental conditions is successfully conducted by rolling up the rollable system around the blood vessel of the swine, the result of which proves the feasibility of a rollable platform as a biomedical device.

## Introduction

Recently, skin-mountable or implantable sensors have been extensively studied for various biomedical applications, such as diagnosis and therapy<sup>1–3</sup>, including brain activity mapping<sup>4,5</sup>, cardiac mapping and therapy<sup>6–8</sup>, and pulse signal measurement<sup>9–11</sup>. In general, to ensure accurate measurement and appropriate treatment, these electronic devices need to be conformally attached to surfaces such as skin or internal organs<sup>12,13</sup>. To achieve conformal contact, various adhesion methods, including mechanical fixturing, the use of adhesive tapes, the use of van der Waals forces, and the use of bioadhesive, have been used<sup>2,14–16</sup>. However, these methods have large

limitations in their application to tubular organs, such as blood vessels or nerves due to their squasy and slippery surfaces with small radii of curvature and narrow contact areas. To measure the biomechanical signals (e.g., pulse or blood pressure) from these tubular organs, it is crucial to develop a device that provides not only sufficient adhesive force to the target surface without causing any damage but also appropriate pressure to detect the signals<sup>15</sup>. Recently, Boutry et al. reported an in vivo arterial-pulse monitoring sensor system implanted in a rat. Although their result suggests a breakthrough in the remote monitoring of biosignals, the sensor system did not obtain a precise pulse signal due to an insufficient adhesive force<sup>17</sup>. A sensor system with insufficient adhesive force cannot collect high-quality data under deformation of the target organ, even if it has high sensitivity. In this respect, providing sufficient gripping force to the target object is one of the crucial issues in biomedical applications. To address this issue, we have adapted the notion of a soft gripper system, which is extensively researched in the field of biorobotics. Studies report various types of soft

Correspondence: Sang Moon Kim ([ksm7852@inu.ac.kr](mailto:ksm7852@inu.ac.kr)) or Daeshik Kang ([dskang@ajou.ac.kr](mailto:dskang@ajou.ac.kr)) or Mansoo Choi ([mchoi@snu.ac.kr](mailto:mchoi@snu.ac.kr))

<sup>1</sup>Global Frontier Center for Multiscale Energy Systems, Seoul National University, Seoul 151-742, Korea

<sup>2</sup>Department of Mechanical and Aerospace Engineering, Seoul National University, Seoul 151-742, Korea

Full list of author information is available at the end of the article.

These authors contributed equally: Gunhee Lee, Yong Whan Choi, Taemin Lee, Kyung Seob Lim

© The Author(s) 2019



**Open Access** This article is licensed under a Creative Commons Attribution 4.0 International License, which permits use, sharing, adaptation, distribution and reproduction in any medium or format, as long as you give appropriate credit to the original author(s) and the source, provide a link to the Creative Commons license, and indicate if changes were made. The images or other third party material in this article are included in the article's Creative Commons license, unless indicated otherwise in a credit line to the material. If material is not included in the article's Creative Commons license and your intended use is not permitted by statutory regulation or exceeds the permitted use, you will need to obtain permission directly from the copyright holder. To view a copy of this license, visit <http://creativecommons.org/licenses/by/4.0/>.

grippers to catch objects with diverse shapes and stiffnesses without causing damage<sup>18,19</sup>. Recently, an advanced soft gripper system with integrated sensors that detect specific signals from the gripped object has been studied<sup>20,21</sup>. However, these grippers are too massive to catch a small object and show limited sensing capability, which proves their inadequacy in the contact-based sensing of tiny movements. Most of all, there is a challenging limitation in combining the two distinct fabrication processes due to the intrinsic differences in the 3D- and 2D-based processes for the gripper<sup>22</sup> and thin-film electronics, respectively.

Herein, we develop nature-inspired rollable electronics, which provide sufficient gripping force to attach to a target object without inducing damage or slipping. In nature, many animals actively control parts of their body in specific shapes with their unique mechanisms for various purposes. For example, some flying bugs utilize their unique folding system to fold their wings at rest and unfold them when flying<sup>23,24</sup>. Mollusks such as squids and octopuses roll their tentacles to grip objects. Moreover, butterflies normally keep their very long but narrow probosces rolled but unroll them when they need to suck nutrients<sup>25</sup>. Inspired by the rolling mechanism of butterflies' probosces and octopuses' tentacles, we have fabricated a rollable platform that can be extremely rolled until the inner diameter of the device reaches  $\sim 1$  mm and can be actively unrolled on demand. We have serially constructed rollable films and flexible electronics since their fabrication processes are 2D-film-based and compatible with each other. On the rollable platform, we have constructed and demonstrated thin-film electronics, including a heater, strain sensor and temperature sensor, which operate in both the unrolled and rolled states. Furthermore, we have demonstrated the rollable platform as a sensor-integrated gripper system by using the rolling force as the gripping force to grip micro-objects and to detect tiny motions of an ant. The rollable platform also measures the expansion and compression of a phantom blood vessel made with a circular rubber tube. Finally, we have conducted *in vivo* pulse wave measurements of a swine's blood vessel with the rollable platform by using its advantage of wrapping and detecting simultaneously.

## Materials and methods

### Fabrication process of rollable platform

The detailed fabrication process is depicted in Figs. S1 and S2. The rollable platform was built by stacking two thin polyimide (PI) films with a polydimethylsiloxane (PDMS) air channel. A chromium (Cr) layer (2 nm) and silicon dioxide ( $\text{SiO}_2$ ) layer (3 nm) with thicknesses of 2 nm were deposited on both sides of the  $12.5 \mu\text{m}$  PI film by a thermal evaporator (Selcos Co., Ltd.). The deposition

of Cr and  $\text{SiO}_2$  enhances the adhesion of the PI film for plasma bonding. We fabricated two types of PI film with deposited Cr and  $\text{SiO}_2$  layers: a PI film with electronic devices and a hole with a radius of 2 mm, where air can be injected (Fig. S2c); a PI film without a hole (Fig. S2a). The dimensions of the two films are 10 mm in width and 70 mm in length. To strongly bond the PI films and make air channels, we introduced a thin PDMS film. The thin PDMS film ( $\sim 1 \mu\text{m}$ ) was formed by spin coating and then cured at  $70^\circ\text{C}$ . After curing the PDMS film, we made a rectangular hole of 4 mm in width and 44 mm in length in the film. The prepared PI film without a hole and the PDMS film with the rectangular hole were  $\text{O}_2$  plasma treated for plasma bonding (CUTE MPR; Femto Science) (Fig. S2b). After bonding, the PI film with the hole was plasma bonded onto the other side of the PDMS film (Fig. S2c). Then, we successfully fabricated a channel system composed of a PI film with electric devices, a PDMS film and a PI film without electronics (Fig. S2d). To roll the channel system with the air channel, we bonded the channel system to a stretched elastomer and then released the elastomer (Figs. S1 and S2e–g). We used a silicone rubber (KEG-2000, Shin-Etsu) as the elastomer. The liquid-type rubber was hardened by heating at  $120^\circ\text{C}$  and applying a pressure of 10 MPa. The thicknesses of the silicone rubber were 40, 70 or  $100 \mu\text{m}$ . Before bonding, the channel system was plasma bonded with  $1 \mu\text{m}$  of PDMS film to enhance the bonding force between the silicone rubber and the PI film (Fig. S2e). Then, the stretched silicone rubber (30, 40, or 50%) and the channel system with the air channel were plasma bonded (Fig. S2f). After bonding, we released the silicone rubber to roll the constructed rollable platform (Figs. S1 and S2g).

### Heater fabrication

The heater was manufactured through a lift-off process. The PI film was spin coated with AZ 5214 and then treated at  $95^\circ\text{C}$  for 1 min. Thereafter, exposure was performed with an aligner for 120 s and developed for 3 min. Then, 3 nm of Cr and 100 nm of Au were deposited using a thermal evaporator (Fig. S4).

### Strain/temperature sensor fabrication

The strain/temperature sensor was fabricated with a three-step photolithography process. The detailed fabrication process is shown in Fig. S5. The electrode for connecting the sensor was fabricated by using the same method used for the heater. To fabricate the strain sensor, photolithography was performed once again, and the sensor was connected to the electrode through alignment. The strain sensor was fabricated by depositing 30 nm of Cr and 30 nm of Pt. Finally, the photolithography process was performed to fabricate the temperature sensor, and the alignment was performed as in the case of fabricating

the strain sensor. Deposition was carried out with thicknesses of 3 nm (Cr) and 30 nm (Pt).

### FE analysis

For verification, the experimental results were compared with the analytical results obtained by FE analysis. FE analysis was performed by a commercial FE analysis program (ABAQUS). In this analysis, a 4-node doubly curved general-purpose shell was used, and the total number of elements was 12,000. As mentioned above, the rollable platform consisted of a PI film, a PDMS, and silicone rubber, and each film material was layer-by-layer stacked. The initial rolled configuration and the rolling behavior of the rollable platform were achieved through the relaxation process after attaching the uniaxial pre-stretched silicone rubber layer. Thus, the initial rolled configuration was affected by the prestretched ratio of the rubber layer. In FE analysis, the mechanical prestrain was implemented and expressed by the product of the artificial thermal coefficient and artificial temperature. In this analysis, it is noted that the implemented prestrain was a logarithmic strain corresponding to the prestrain ratio of the silicone rubber sheet. In addition, the self-contact condition of the rollable sheet was not considered for simplification of the FE analysis.

### Physical analysis

Magnified optical images were obtained using an optical microscope (Olympus IX70, Japan). Scanning electron microscopy images were obtained by using a field emission scanning electron microscope (Carl Zeiss) at an acceleration voltage of 10.0 kV to observe the morphologies of the surfaces of the samples.

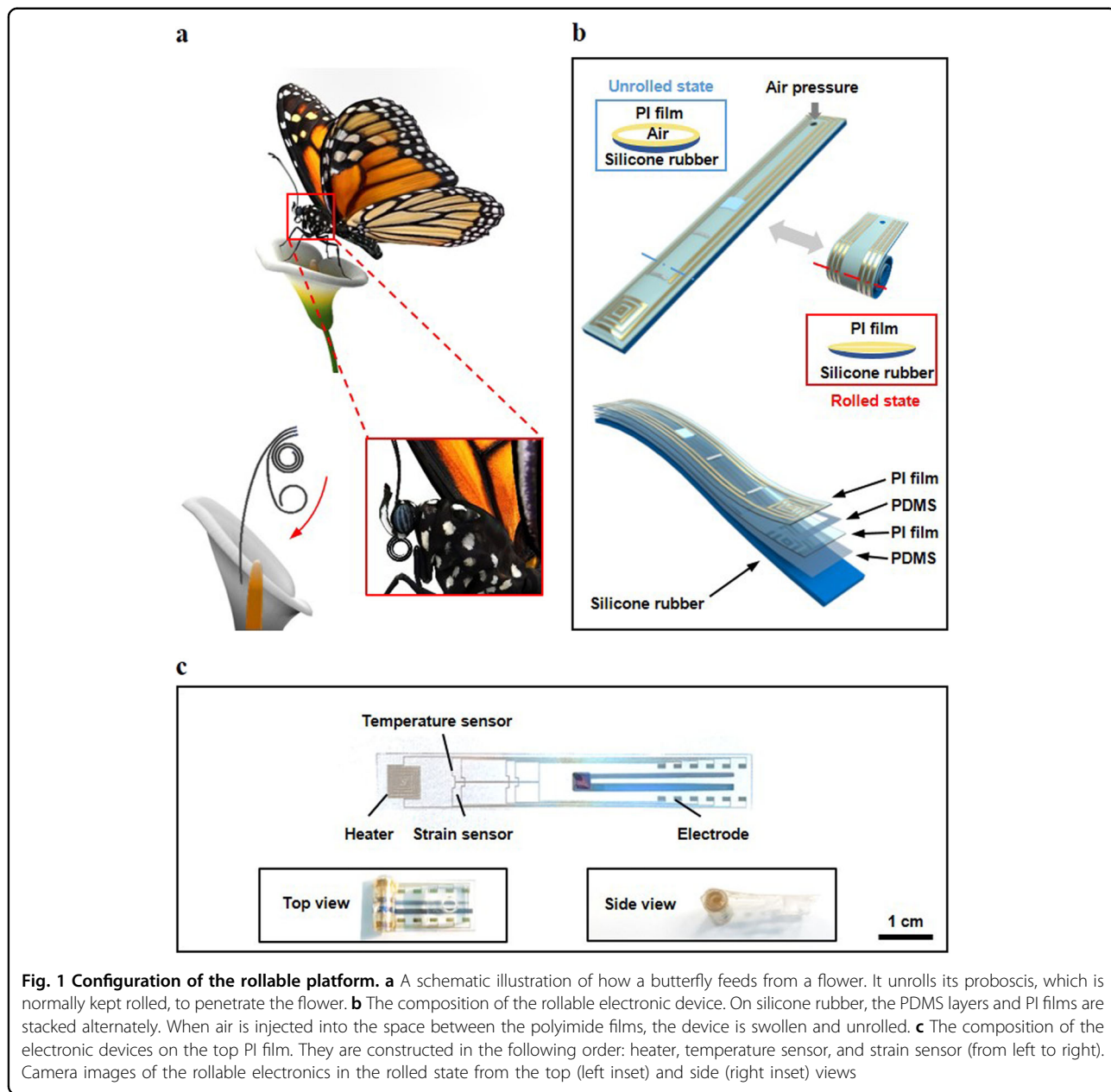
### Animal preparation and procedure

The present animal study was approved by the Ethics Committee of Chonnam National University Medical School and Chonnam National University Hospital (CNU IACUC-H-2018-52) and conformed to the Guide for the Care and Use of Laboratory Animals published by the United States National Institutes of Health (NIH Publication No. 85–23, revised 1996). The study animals were two Yorkshire X Landrace F1 crossbred castrated male swine weighing 20–25 kg. On procedure day, the swine were anesthetized with zolazepam and tiletamine (2.5 mg/kg; Zoletil50®, Virbac, Caros, France), xylazine (3 mg/kg; Rompun®, Bayer AG, Leverkusen, Germany), and azaperone (6 mg/kg; Stresnil®, Janssen-Cilag, Neuss, Germany). Because zolazepam and tiletamine are weak muscle relaxants, xylazine was added. Azaperone was used to extend the anesthesia. The animals received supplemental oxygen via endotracheal intubation throughout the procedure by isoflurane inhalation (2%). The anesthetic depth was clinically monitored on the

basis of the cessation of movement, eye position, loss of muscular tone, and absence of palpebral, and pedal reflexes<sup>26,27</sup>. The right and left superficial femoral arteries were exposed surgically after a subcutaneous injection of 2% lidocaine. A 4 Fr sheath was inserted into the right superficial femoral artery, and the aortic pressure and wave were continuously recorded with the RadiAnalyzer™ (Abbott Vascular, Santa Clara, CA, USA). Continuous hemodynamic and surface electrocardiographic monitoring was performed throughout the procedure<sup>28</sup>. Simultaneously, a rollable sensor was wrapped around the left superficial femoral artery to record the pulse wave. To evaluate the pulse wave consistency in variable situations, we conducted signal recordings after epinephrine injection to elevate the cardiac output and potassium chloride injection via an artery sheath for euthanization.

### Results and discussion

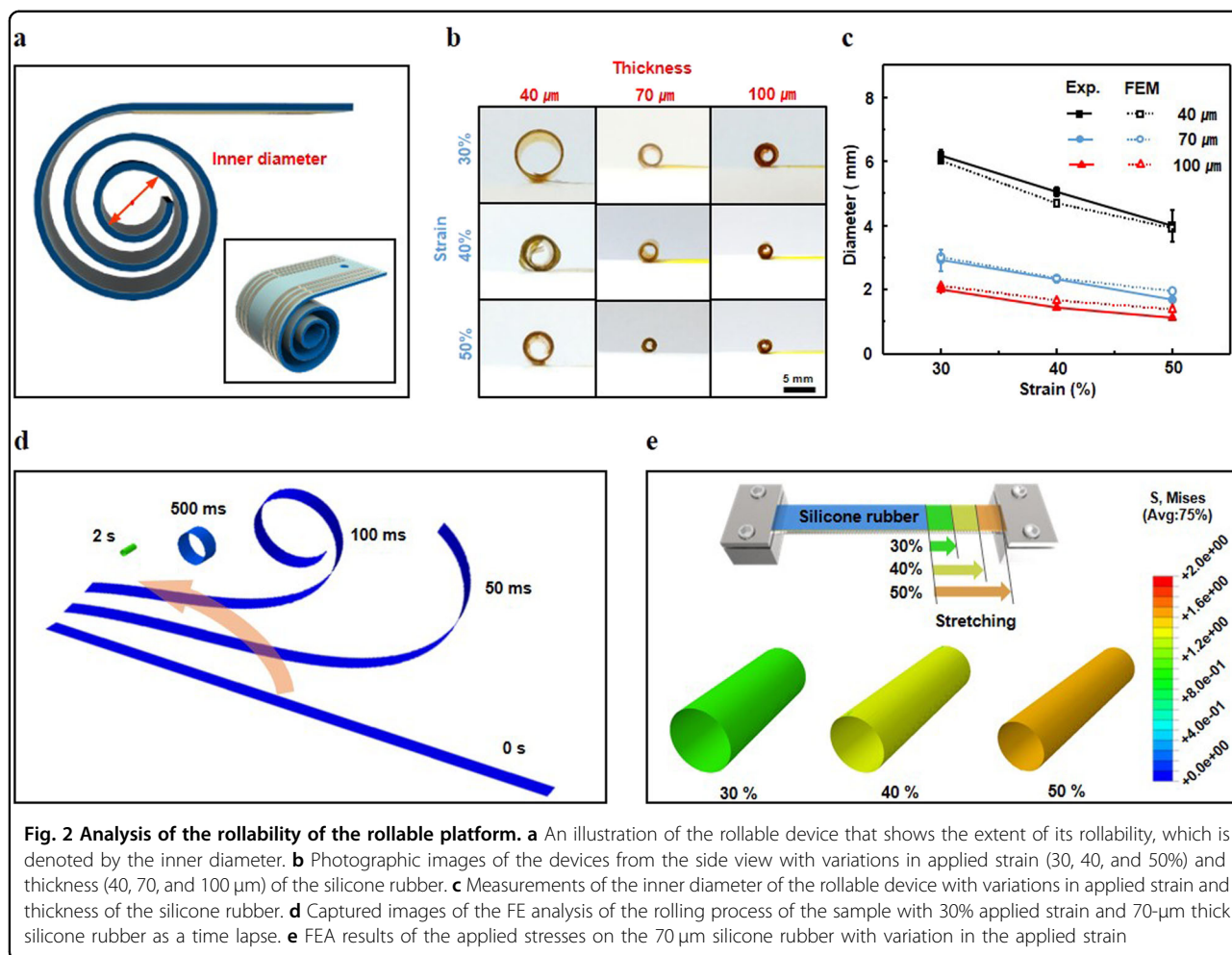
Figure 1a shows a schematic illustration of how *Lepidoptera* feed from flowers in nature. They normally have their very long but narrow probosces rolled up but unroll them to take in nutrients<sup>29</sup>. Although the opening of a flower is narrow and the target nutrients are located deep inside the flower, *Lepidoptera* can stretch out their probosces to easily reach food sources. The rolling and unrolling movements of the probosces of *Lepidoptera* are conducted through a hydraulic drive system that uses elastic parts and musculature<sup>25,30,31</sup>. The rolling of the proboscis is driven by its elasticity and decreasing pressure in its channel. On the other hand, the proboscis becomes unrolled as the pressure in the channel increases and as the muscle contracts. Inspired by the rolling and unrolling behavior of *Lepidoptera*, we have developed a rollable platform that consists of two main parts: a channel system and an elastomeric substrate. The former is composed of multilayers, including PDMS and PI films. These films are stacked and bonded alternately via plasma bonding, as shown in Fig. 1b. The PDMS layer, with a thickness of approximately 1 μm, is located between the PI films. This construction results in a small void space where air can be injected, which is necessary to unroll the device. The latter part is a silicone rubber substrate, which is initially stretched and bonded to the surface of the PI film. This layer is responsible for rolling the platform, as illustrated in the inset of Fig. 1b. If the prestretched silicone rubber is bonded to the PI film and then released, it shrinks and generates a bending moment on the entire film. The generated moment causes the entire film to be rolled to a specific radius, depending on the degree of prestrain. Thus, the rollable electronics essentially maintain the rolled state. The unrolling behavior of the rollable electronics is driven by pneumatic pressure. The detailed manufacturing process of the rollable electronics is described in the Experimental Section and in Fig. S1. The



platform is capable of being stretched by injecting air through the air channels between the PI films. This procedure can occur because the pressure of the injected air keeps the channels in a swollen form (Fig. 1b). By using this mechanism, the device can be rolled and unrolled repeatedly and actively.

As the rollability of the platform is physically affected by the stress of the silicone rubber, its strain and thickness are varied to investigate the effect of the stress. The strain is defined as the change in length after stretching divided by the original length ( $\epsilon = \Delta L/L$ ). The inner diameter of the rollable electronics is used as the index of its rollability, as shown in Fig. 2a. Figure 2b

shows photographic images of the device from the side view with variations in the applied strain (30, 40, and 50%) and thickness (40, 70, and 100  $\mu\text{m}$ ) of the silicone rubber. As expected, the inner diameter of the film almost linearly decreases as the applied strain increases due to the elevated recovery force of the elastic film. As the film thickness increases, the inner diameter decreases due to the increased contraction force of the layer. In the case of an applied strain of 50% and a thickness of 100  $\mu\text{m}$ , the inner diameter of the device is  $\sim 1$  mm. In this case, as observed above, the area of the film in the rolled state is reduced to 1/50 compared to that in the unrolled state. To verify the tendency of rollability with



the variation in strain and thickness of the silicone rubber layer, we conducted a finite element (FE) analysis. The results were acquired through the relaxation process after attaching the uniaxial prestretched silicone rubber layer. Details regarding the simulation method are presented in the Experimental Section of this paper. The experimental and simulation data are in good agreement, as shown in Fig. 2c. Figure 2d shows that the platform is rolled to a very small size over time. The platform is initially rolled from one end of the film and turns around at 500 ms, showing a gradual decrease, and the final shape appears at 2 s. The rolling process progresses until the restoring stress of the silicone rubber and flexural strength of the PI film reach equilibrium. Movie clips in the Supplementary information show the entire rolling process. In Fig. 2e, the captured images of FE analysis with variations in the applied strain for the 70- $\mu\text{m}$  thick silicone rubber show that the inner diameter of the rolled film decreases as the strain of the silicone rubber film increases. As shown in Fig. S3, which presents the von Mises stress of the silicone

rubber in all cases, the inner diameter of the rollable electronics decreases as the prestrain increases.

Based on the fundamental study of the mechanism, we have constructed rollable electronics that can be actively controlled. The rollable electronics can alter their geometrical shape to be rolled or unrolled on demand. Figure 1c presents a photographic image of several electronic devices on the rollable platform in its unrolled state. The devices shown here consist of four independent functional components, namely, a heater, a temperature sensor, a crack-based strain sensor and an electrode, in order from left to right. A detailed description of the operation of each constructed electronic device is given in Fig. 3. We now investigate the feasibility of each electronic part when it is rolled and unrolled. The detailed manufacturing process of the electronics is described in the Experimental Section and in Figs. S4 and S5. Figure 3a shows photographic images of the heater, with 5 V applied by a voltage source. The heater was designed in the shape of a maze pathway with a thin and narrow electrode. The applied current induced heat, and then the temperature of the

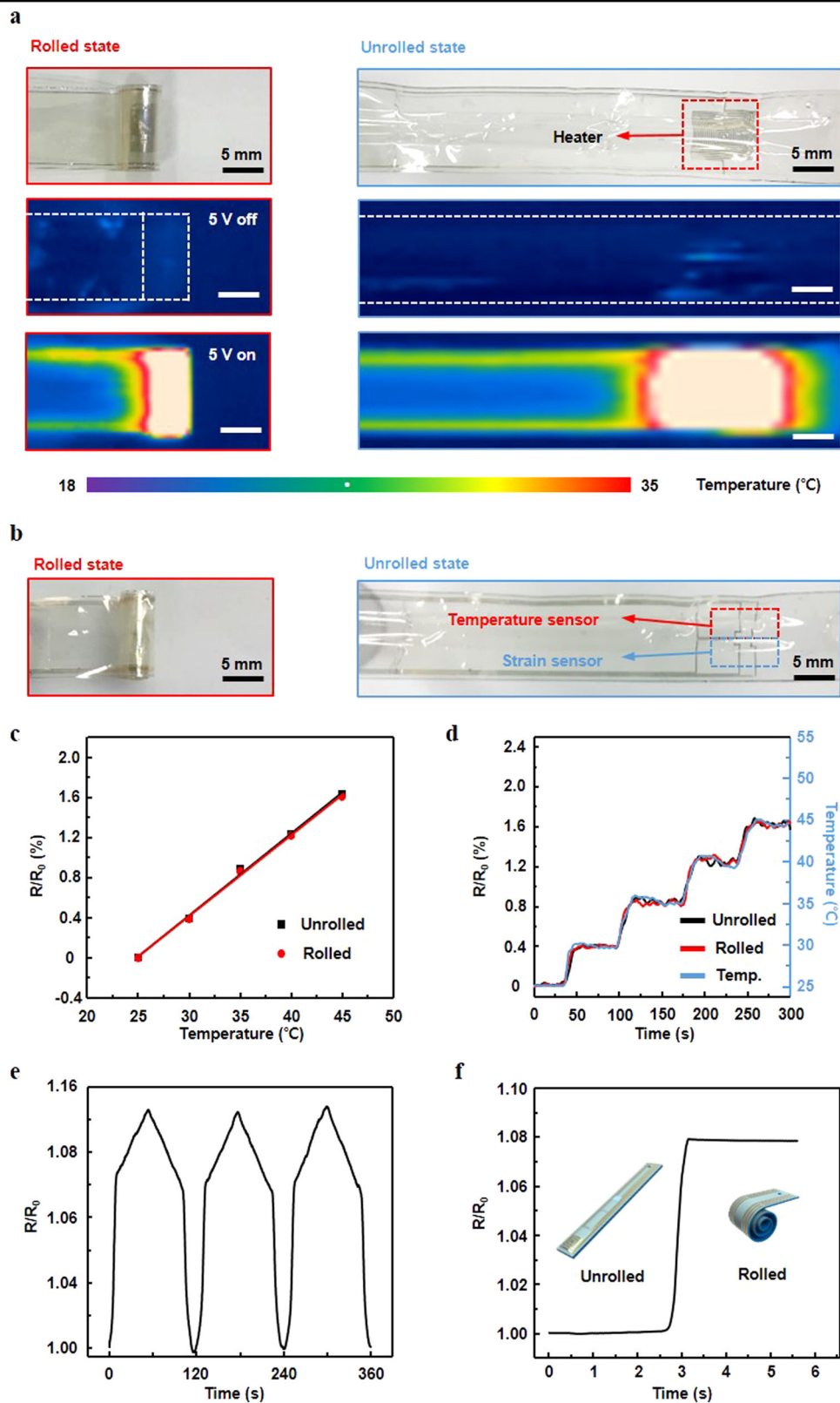


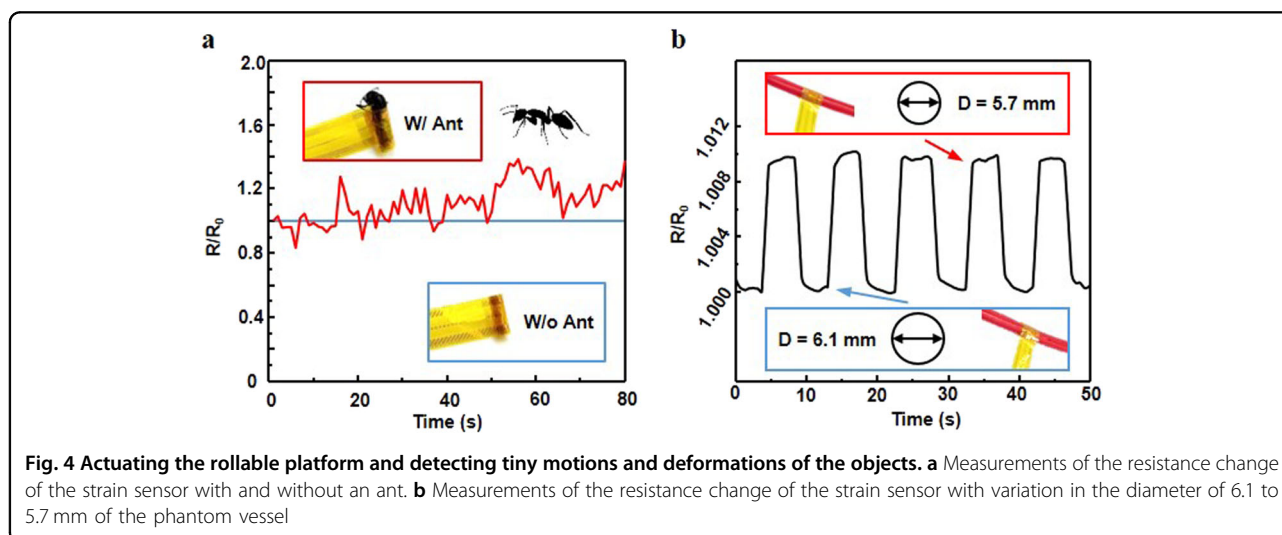
**Fig. 3** Operation of various electronic devices on the rollable platform. **a** Photographic and thermal images of the heater in its unrolled and rolled states. Thermal images of the heater show the temperature distribution when currents are applied. **b** Photographic images of the temperature and strain sensor in their unrolled and rolled states. **c, d** Measurements of the resistance change of the temperature sensor with the variation in temperature in its rolled and unrolled states. **e** The graph of normalized resistance variance of the strain sensor with an applied strain of 2%. **f** Measurements of the resistance change of the strain sensor in its rolled and unrolled states

heater reached 35 °C. As shown in Fig. 3a, the heater was normally operated even in the rolled state, showing comparable a temperature distribution in the unrolled state. The temperature sensor in Fig. 3b, composed of a platinum resistor, exhibits a linear response with a variation in temperature from 25 to 45 °C in both the rolled and unrolled states (Fig. 3c). The response times in both states were analogous to those in the unrolled state (Fig. 3d). Figure 3e shows the change in resistance of the crack-based sensor between repeated applied strains of 0–2%<sup>9,32</sup>. The resistance of the sensor in the rolled state increases compared to that in the unrolled state due to the gradual disconnection of nanoscale crack junctions (Fig. 3f). As the rolling progresses, the inner diameter of the platform decreases, which increases the resistance of the sensor. Based on the results, the crack-based strain sensor on the rollable platform is applied to the measurement of the curvature of circular target structures.

We now demonstrate the rollable soft gripper mounted with crack sensors, which can detect minute movements or vibrations of an insect. Generally, when a rigid gripper grasps micro bio-objects such as insects with strong force, it may cause some serious damage to the gripped objects<sup>33–35</sup>. With rollable electronics on soft polymeric materials, we can achieve nondamaging manipulations of the micro bio-objects. Figure 4a shows that an ant is well gripped using the rollable soft gripper. To grip the ant, we unrolled the platform by applying air pressure and then decreased the pressure to wrap around and hold the ant. After gripping the ant with the gripper, we successfully measured the resistance variation of the crack sensor, which was induced by the tiny movement of the gripped ant. The results imply that our rollable electronic device can be successfully applied to not only a soft gripper for manipulating micro bio-objects but also a device that detects their tiny motions and vibrations. We measured

the extent of expansion of a phantom blood vessel with the crack sensor mounted on the rollable electronics. The platform can make conformal contact with the phantom blood vessel, and contraction and expansion of the vessel were well measured. The diameter of the phantom blood vessel was 5.7 mm before deformation and 6.1 mm after deformation induced by air pressure in the vessel. The resistance of the sensor changed stably and repeatedly when we applied and removed the air pressure five times (Fig. 4b). This result implies that our device can be extensively applied to biomedical research, especially for the precise measurement of blood pressure and pulse wave velocity or for direct contact-based drug delivery<sup>36–39</sup>.

To confirm the practical effectiveness of our device, we demonstrate an *in vivo* biomedical application. We conducted pulse wave measurements with rollable electronics by wrapping a superficial femoral artery of a swine in the rolled state. Figure 5a shows illustrations of the experimental setup used to detect the pulse wave of the swine. To conduct the *in vivo* test, both femoral artery vessels in the left and right legs of the swine were opened up. Then, a sheath for measuring the intravascular pressure of a conventional system was inserted into the vessel of the right leg, and the strain sensor on the rollable electronics was rolled up around the vessel in the left leg to detect the pulse wave passing through the artery vessels (Fig. 5b). The conventional pulse wave measuring device was used as a reference. As shown in Fig. 5c–e, to verify the effectiveness of the gripping force of the rollable electronics in detecting the pulse wave of the swine, the pulse wave signals were compared with the conventional measurement data in the following three cases: (i) when the rollable electronics gripped the artery tightly (rolled state), (ii) when it was in passive contact with the artery without rolling (unrolled state), and (iii) when it was wrapped around the artery and fixed (semi-rolled state). Figure 5f, g



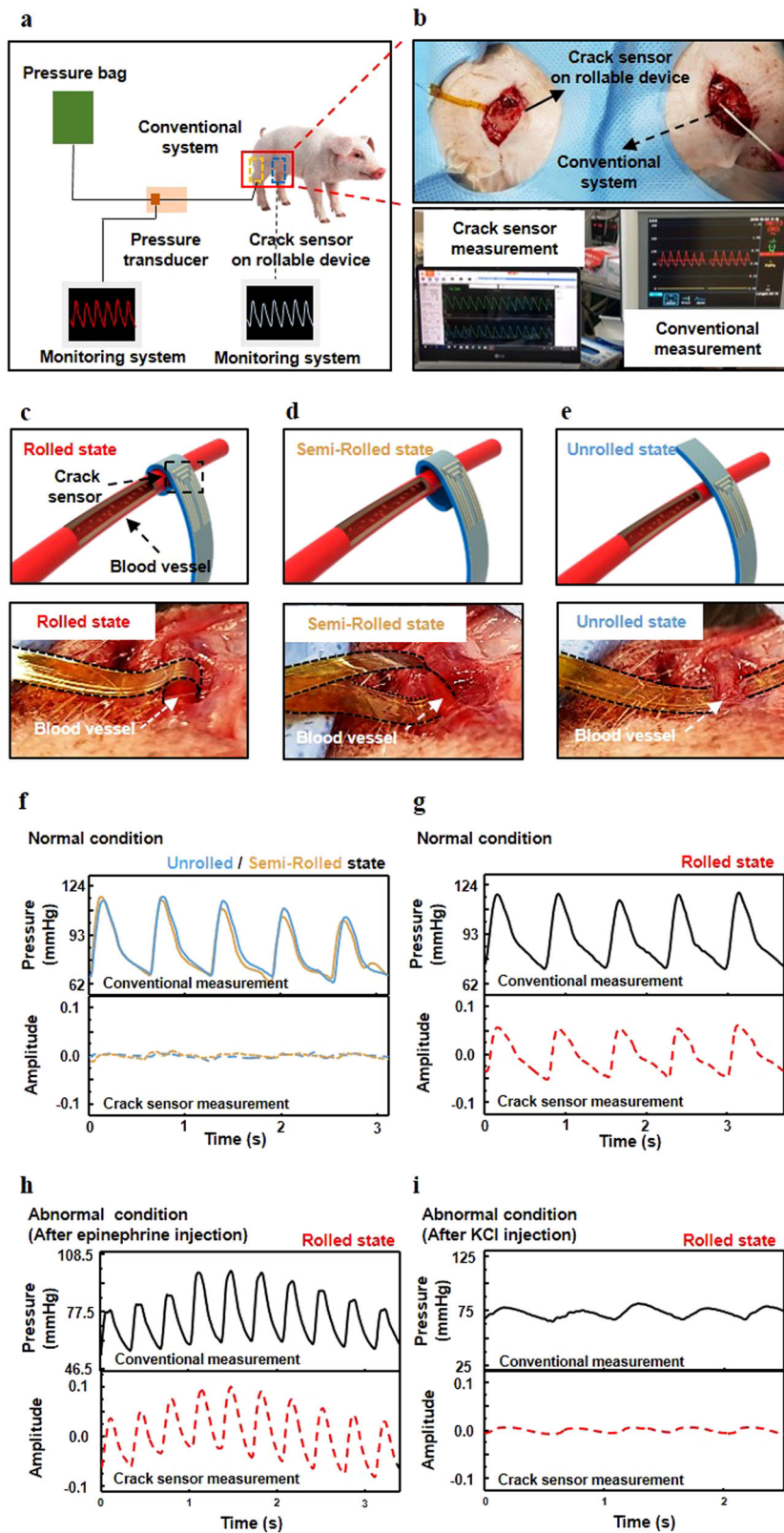


Fig. 5 (See legend on next page.)



(see figure on previous page)

**Fig. 5 In vivo animal test to detect the pulse waves of swine with rollable electronics.** **a** Schematic illustration of two types of systems for pulse wave detection. **b** Photographic images of the conventional measurement system and crack-based strain sensor on the rollable platform, which are mounted on the blood vessels of a swine. **c–e** Schematic illustrations and photographic images of the rollable device wrapped around a blood vessel in its **(c)** rolled, **(d)** semi-rolled, and **(e)** unrolled state. **f, g** Pulse wave signals of the swine blood vessels through a sheath-based conventional monitoring system and our device in its **(f)** unrolled, semi-rolled and **(g)** rolled states under normal conditions. **h, i** Pulse wave signals of the swine blood vessels with our device rolled around them under abnormal conditions **(h)** after epinephrine injection and **(i)** after KCl injection

shows the measurement results of pulse waves according to the three different detection methods. The results show that the detection performance of the rolled state is significantly different from that of the unrolled state. In the rolled state, the measured signals were analogous when compared to the signal measured by the sheath-based conventional monitoring system. In contrast, in the unrolled state and semi-rolled state, the measured signals were unclear and did not change much in response to the pulse wave change of the swine (Fig. 5f). The pulse wave signals were measured well in the rolled state since the rollable platform gripped and fixed the artery with the proper pressure. On the other hand, in the unrolled state and semi-rolled state, the platform was in contact with the artery but could not stick to or grip the artery well, inducing unclear signal detection. Furthermore, to verify the ability to detect signals of our devices under various hemodynamic conditions, we checked the pulse wave responses in the other two cases and compared them with the signals from the conventional monitoring system (Fig. 5h, i). We injected epinephrine, which is a nonselective agonist of all adrenergic receptors, to raise the heart rate and blood pressure of the swine and potassium chloride to induce cardiac arrhythmia, such as ventricular fibrillation and heart blockage, to decrease the blood pressure. As expected, the rollable device successfully detected the signals under the various hemodynamic conditions. Considering the conformability, size and measurement accuracy of the device, the rollable device can be used for invasive and noninvasive blood pressure monitoring under various conditions. The device is also applicable to blood vessels of various sizes, from the arteriole to the aorta, with controllability of its shape and size. Most of all, continuous monitoring of the blood pressure both inside and outside a blood vessel as well as at the skin can be performed. Our device will be used in a wide range of applications, including portable, long-term and real-time biomonitoring systems with the aid of wireless communication technology and the application of bioabsorbable material.

## Conclusions

We have developed rollable electronics composed of polymeric multilayers of PDMS, PI, and silicone rubber inspired by the rolling mechanism of the proboscis of a butterfly. The prestretched silicone rubber bonded to the

PI film induces the rolling of the platform, and injecting air into the void space between the adjacent PI films unrolls the platform from its rolled state. This rolling mechanism offers a uniform stress distribution on the substrate, which prevents failures of the electric connection of the device with the highly concentrated stress at the folded edge. The degree of rolling can be managed by varying the thickness of the elastomeric film and strain applied to the film. This result has been confirmed through experiments and FE analysis studies. On the rollable electronics, we have constructed thin-film electronics, including a heater, strain sensor and temperature sensor, which operate normally in both the rolled and unrolled states. The integrated system can grip micro bio-objects and detect tiny motions of the objects. Furthermore, we have successfully conducted in vivo animal tests to detect pulse wave signals of the superficial femoral artery of swine using the rollable electronics. With the advantages of our rollable electronics, they can be applied to broad research fields, including biomedical electronic systems, in the near future.

## Acknowledgements

G. Lee, Y. W. Choi, T. Lee, and K. S. Lim contributed equally to this work. M. Choi acknowledges financial support from the Global Frontier R&D Program of the Center for Multiscale Energy Systems (2012M3A6A7054855) funded from the National Research Foundation (NRF) of Korea. D. Kang, S. M. Kim and H. K. Kim acknowledge financial support from the Basic Science Research Program through the National Research Foundation of Korea (NRF) funded by the Ministry of Science, ICT & Future Planning (2016R1C1B1009689, 2019R1C1C1006392, 2019R1H1A1080221, 2019R1A2C1090056, and 2017R1C1B5017469). D. Kang acknowledges financial support from the new faculty research fund of Ajou University and the Ajou University research fund. This material is based upon work supported by the Ministry of Trade, Industry & Energy (MOTIE, Korea) under Industrial Technology Innovation Program, No. 20000512, "Development of Task Planning, Gripping and Manipulation Technologies of Deformable Objects based on Machine Learning for Manufacturing and Logistical Process".

## Author details

<sup>1</sup>Global Frontier Center for Multiscale Energy Systems, Seoul National University, Seoul 151-742, Korea. <sup>2</sup>Department of Mechanical and Aerospace Engineering, Seoul National University, Seoul 151-742, Korea. <sup>3</sup>Division of Mechanical Convergence Engineering, College of MICT Convergence Engineering, Silla University, Busan 46958, Republic of Korea. <sup>4</sup>Futuristic Animal Resource and Research Center, Korea Research Institute of Bioscience and Biotechnology, Ochang 28116 Chungbuk, Korea. <sup>5</sup>Department of Mechanical Engineering, Ajou University, San 5, Woncheon-dong, Yeongtong-gu, Suwon 443-749, Republic of Korea. <sup>6</sup>Department of Internal Medicine and Cardiovascular Center, Chosun University Hospital, University of Chosun College of Medicine, Gwangju, Korea. <sup>7</sup>Department of Internal Medicine and Cardiovascular Center, Seoul National University Hospital, Seoul, Korea. <sup>8</sup>Institute on Aging, Seoul National University, Seoul, Korea. <sup>9</sup>Division of Cardiology of Chonnam National University Hospital, Gwangju, Korea.

<sup>10</sup>Department of Nanobiomedical Science & BK21 PLUS Global Research Center for regenerative Medicine, Dankook University, Cheonan 330-714, Republic of Korea. <sup>11</sup>Department of Mechanical Engineering, Incheon National University, Incheon 406-772, Korea. <sup>12</sup>Department of Internal Medicine and Cardiovascular Center, Chonnam National University Hospital, Gwangju, Korea

#### Conflict of interest

The authors declare that they have no conflict of interest.

#### Publisher's note

Springer Nature remains neutral with regard to jurisdictional claims in published maps and institutional affiliations.

**Supplementary information** is available for this paper at <https://doi.org/10.1038/s41427-019-0169-z>.

Received: 5 April 2019 Revised: 6 August 2019 Accepted: 9 September 2019.

Published online: 22 November 2019

#### References

- Vaddiraju, S., Tomazos, I., Burgess, D. J., Jain, F. C. & Papadimitrakopoulos, F. Emerging synergy between nanotechnology and implantable biosensors: a review. *Biosens. Bioelectron.* **25**, 1553–1565 (2010).
- Kim, D.-H. et al. Epidermal electronics. *Science* **333**, 838–843 (2011).
- Jeong, Y. R. et al. A skin-attachable, stretchable integrated system based on liquid GalnSn for wireless human motion monitoring with multi-site sensing capabilities. *NPG Asia Mater.* **9**, e443 (2017).
- Viventi, J. et al. Flexible, foldable, actively multiplexed, high-density electrode array for mapping brain activity in vivo. *Nat. Neurosci.* **14**, 1599 (2011).
- Alivisatos, A. P. et al. Nanotools for neuroscience and brain activity mapping. *ACS Nano*. **7**, 1850–1866 (2013).
- Kim, D.-H. et al. Electronic sensor and actuator webs for large-area complex geometry cardiac mapping and therapy. *Proc. Natl Acad. Sci.* **109**, 19910–19915 (2012).
- Kim, D.-H. et al. Materials for multifunctional balloon catheters with capabilities in cardiac electrophysiological mapping and ablation therapy. *Nat. Mater.* **10**, 316 (2011).
- Kim, D.-H., Lu, N., Ghaffari, R. & Rogers, J. A. Inorganic semiconductor nanomaterials for flexible and stretchable bio-integrated electronics. *NPG Asia Mater.* **4**, e15 (2012).
- Kang, D. et al. Ultrasensitive mechanical crack-based sensor inspired by the spider sensory system. *Nature* **516**, 222 (2014).
- Cianchetti, M., Laschi, C., Menciasci, A. & Dario, P. Biomedical applications of soft robotics. *Nat. Rev. Mater.* **1**, 143–153 (2018).
- Roche, E. T. et al. Soft robotic sleeve supports heart function. *Sci. Transl. Med.* **9**, eaf3925 (2017).
- Choi, S. et al. Highly conductive, stretchable and biocompatible Ag–Au core–sheath nanowire composite for wearable and implantable bioelectronics. *Nat. Nanotechnol.* **13**, 1048–1056 (2018).
- Miyamoto, A. et al. Inflammation-free, gas-permeable, lightweight, stretchable on-skin electronics with nanomeshes. *Nat. Nanotechnol.* **12**, 907 (2017).
- Mahdavi, A. et al. A biodegradable and biocompatible gecko-inspired tissue adhesive. *Proc. Natl Acad. Sci.* **105**, 2307–2312 (2008).
- Chen, X., Assadsangabi, B., Hsiang, Y. & Takahata, K. Enabling angioplasty-ready “Smart” Stents to detect in-stent restenosis and occlusion. *Adv. Sci.* **5**, 1700560 (2018).
- Lee, H., Lee, B. P. & Messersmith, P. B. A reversible wet/dry adhesive inspired by mussels and geckos. *Nature* **448**, 338 (2007).
- Boutry, C. M. et al. Biodegradable and flexible arterial-pulse sensor for the wireless monitoring of blood flow. *Nat. Biomed. Eng.* **3**, 47 (2019).
- Laschi, C., Mazzolai, B. & Cianchetti, M. Soft robotics: technologies and systems pushing the boundaries of robot abilities. *Sci. Robot.* **1**, eaah3690 (2016).
- Rus, D. & Tolley, M. T. Design, fabrication and control of soft robots. *Nature* **521**, 467 (2015).
- Wall, V., Zöllner, G. & Brock, O. In *2017 IEEE International Conference on Robotics and Automation (ICRA)*. 4965–4970 (IEEE).
- Zhao, H., O'Brien, K., Li, S. & Shepherd, R. F. Optoelectronically innervated soft prosthetic hand via stretchable optical waveguides. *Sci. Robot.* **1**, eaai7529 (2016).
- Truby, R. L. et al. Soft somatosensitive actuators via embedded 3D printing. *Adv. Mater.* **30**, 1706383 (2018).
- Faber, J. A., Arrieta, A. F. & Studart, A. R. Bioinspired spring origami. *Science* **359**, 1386–1391 (2018).
- Saito, K., Nomura, S., Yamamoto, S., Niiyama, R. & Okabe, Y. Investigation of hindwing folding in ladybird beetles by artificial elytron transplantation and microcomputed tomography. *Proc. Natl Acad. Sci.* **114**, 5624–5628 (2017).
- Zhou, X. & Zhang, S. Manipulate the coiling and uncoiling movements of Lepidoptera proboscis by its conformation optimizing. Preprint at: arXiv:1311.1555 (2013).
- Vilahr, G. et al. Protective effects of ticagrelor on myocardial injury after infarction. *Circulation* **134**, 1708–1719 (2016).
- Kim, H. K. et al. Effects of ticagrelor on neointimal hyperplasia and endothelial function, compared with clopidogrel and prasugrel, in a porcine coronary stent restenosis model. *Int. J. Cardiol.* **240**, 326–331 (2017).
- Lee, J. M. et al. Influence of local myocardial damage on index of microvascular resistance and fractional flow reserve in target and nontarget vascular territories in a porcine microvascular injury model. *JACC Cardiovasc. Interv.* **11**, 717–724 (2018).
- Krenn, H. W. Feeding mechanisms of adult Lepidoptera: structure, function, and evolution of the mouthparts. *Annu. Rev. Entomol.* **55**, 307–327 (2010).
- Krenn, H. W. Functional morphology and movements of the proboscis of Lepidoptera (Insecta). *Zoomorphology* **110**, 105–114 (1990).
- Bänziger, H. Extension and coiling of the lepidopterous proboscis—a new interpretation of the blood-pressure theory. *Mitt. Schweiz. Entomol. Ges.* **43**, 225–239 (1971).
- Lee, T. et al. Crack-based strain sensor with diverse metal films by inserting an inter-layer. *RSC Adv.* **7**, 34810–34815 (2017).
- Paek, J., Cho, I. & Kim, J. Microrobotic tentacles with spiral bending capability based on shape-engineered elastomeric microtubes. *Sci. Rep.* **5**, 10768 (2015).
- Shepherd, R. F. et al. Multigait soft robot. *Proc. Natl Acad. Sci.* **108**, 20400–20403 (2011).
- Rothmund, P. et al. A soft, bistable valve for autonomous control of soft actuators. *Sci. Robot.* **3**, 7986 (2018).
- Webb, R. C. et al. Epidermal devices for noninvasive, precise, and continuous mapping of macrovascular and microvascular blood flow. *Sci. Adv.* **1**, e1500701 (2015).
- Shin, K.-H., Moon, C.-R., Lee, T.-H., Lim, C.-H. & Kim, Y.-J. Flexible wireless pressure sensor module. *Sens. Actuators A Phys.* **123**, 30–35 (2005).
- Lee, J. et al. Transfer-molded wrappable microneedle meshes for perivascular drug delivery. *J. Controlled Release* **268**, 237–246 (2017).
- Reeder, J. et al. Mechanically adaptive organic transistors for implantable electronics. *Adv. Mater.* **26**, 4967–4973 (2014).